Control of Pipe Cutting Robot: A More Effective Method

Quoc Bao DIEP

Faculty of Electrical Engineering and Computer Science, VSB–Technical University of Ostrava, 17. listopadu 15, 708 33 Ostrava, Czech Republic

diepquocbao@gmail.com

(Received: 04-August-2017; accepted: 04-October-2017; published: 30-November-2017)
DOI: http://dx.doi.org/10.25073/jaec.201712.82

Abstract. *This paper presents a pipe cutting Robot system with two different cutting methods: the method with the end-effector moves on cutting path and direction while the stationary pipe and the method with the end-effector moves on a straight line while the rotating pipe to create the desired cutting path and direction. The cutting trajectory are described, the Robot model is constructed, solving the inverse kinematics, planning the trajectory of motion, simulating and controlling Robot in Matlab, and designing the experimental Robot to verify. The results of the two methods are compared to point out a better one. This research builds up an important foundation for choosing an effective method for pipe cutting Robot in industry.*

Keywords

Cutting robot, inverse kinematics, pipe cutting, robot control, trajectory planning.

1. Introduction

In industry, gases and liquids are transported daily by pipelines and these pipeline systems paired together in a complex way. To create them, the steel pipes are cut and welded together. However, this is not simple because there are complex joints that require cutting and welding paths to be complicated in which the trajectory and direction change continuously. With that requirement, conventional tools cannot be implemented and the application of robots is necessary.

The use of robot for cutting pipe has become very popular in the world. In Vietnam, this technique has not yet been widely applied, and there are few scientific publications in this field.

In [1], the authors mentioned a Delta Robot for cutting high-speed laser with the numerous advantages of robot: higher stiffness, fewer joints, the ability of transporting heavier loads, and higher accuracy. The main drawback is the small workspace, and this paper also does not mention much about the application of Delta Robot to cut steel pipes.

In [2], the authors presented a pipe cutting technique that included a pipe cutting Robot that the robot arm moves and the pipe is stationary during cutting. The authors successfully builds 3D simulation and experimental model, solving the inverse kinematics, planning the trajectory as well as designs Robot controller. The results of simulated and experimental errors are provided. However, the authors only stopped at the method of the end-effector moves while the stationary pipe without mentioning their coordinated motion.

In this paper, the author presents another method of cutting pipe more effectively with a 6 degrees of freedom pipe cutting Robot, consisting of 5 degrees of freedom robot arm and the

degree of freedom created by the rotating motion of a pipe. With this method, the end-effector will only move on a straight line, and the pipe will rotate in conjunction with the movement of the end-effector to create cutting path in reality. This result is compared with the results in [2] to point out that this cutting method is better than the cutting method in [2].

2. Pipe Cutting Problem

The cutting paths and cutting directions can happen many cases, depending on pipeline assembly position and welding conditions. This paper will focus on Hyperbolic Paraboloid Pringles; a common path is created by two intersecting pipes as shown in Fig. 1.

2.1. Cutting Path

In coordinate frame $\{-1\}$, place pipes R_1 and R_2 which have center lines coincident with Z_{-1} axis, each pipe equation is given by Eq. (1):

$$\begin{cases} x_n^2 + y_n^2 = R_n^2, \\ -\frac{1}{2}L_n \le z_n \le \frac{1}{2}L_n, \end{cases} \tag{1}$$

where

- L, R: the length and radius of two pipes,
- x, y, z: coordinates of two pipes and
- $n = 1$: pipe R_1, $n = 2$: pipe R_2.

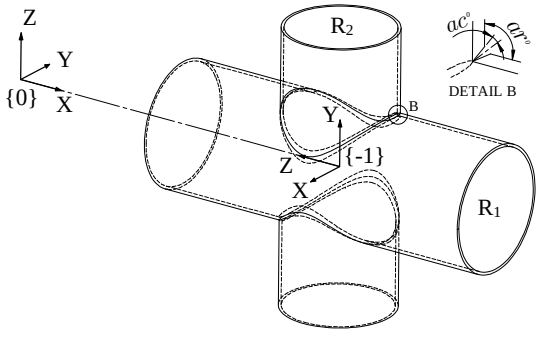

Fig. 1: The intersection of two pipes.

When turning pipe R_2 an angle ar° around X_{-1} axis (for example 90°, see Fig. 1), we have Eq. (2):

$$\begin{bmatrix} x_2' \\ y_2' \\ z_2' \end{bmatrix} = \begin{bmatrix} 1 & 0 & 0 \\ 0 & c_{ar} & -s_{ar} \\ 0 & s_{ar} & c_{ar} \end{bmatrix} \begin{bmatrix} x_2 \\ y_2 \\ z_2 \end{bmatrix}, \tag{2}$$

where

- ar: angle between R_1 and R_2 and
- s_{ar}: $\sin ar$, c_{ar}: $\cos ar$.

Based on Eq. (1) and Eq. (2), we obtain the equation of pipe R_2 after turning ar° as Eq. (3):

$$\begin{cases} x_2^2 + (y_2 c_{ar} - z_2 s_{ar})^2 = R_2^2, \\ -\frac{1}{2}L_2 \le y_2 s_{ar} + z_2 c_{ar} \le \frac{1}{2}L_2. \end{cases} \tag{3}$$

From Eq. (1), Eq. (2) and Eq. (3), we have the locus of the intersection of two pipes as Eq. (4):

$$\begin{cases} x^2 + y^2 = R_1^2, \\ x^2 + (yc_{ar} - zs_{ar})^2 = R_2^2. \end{cases} \tag{4}$$

Assuming that $R_1 \ge R_2$, set:

$$\begin{cases} R_2 s_\varphi = x, \\ R_2 c_\varphi = yc_{ar} - zs_{ar}, \end{cases} \tag{5}$$

where $0 \le \varphi \le 2\pi$, s_φ: $\sin\varphi$, c_φ: $\cos\varphi$.

Based on Eq. (4) and Eq. (5), we obtain the locus of the intersection of two pipes in the coordinate frame $\{-1\}$ as Eq. (6), Eq. (7) and Eq. (8):

$$x = R_2 s_\varphi, \tag{6}$$

$$y = \pm\sqrt{R_1^2 - (R_2 s_\varphi)^2}, \tag{7}$$

$$z = \frac{-R_2 c_\varphi \pm c_{ar}\sqrt{R_1^2 - (R_2 s_\varphi)^2}}{s_{ar}}. \tag{8}$$

Set up the coordinate frame $\{0\}$ so that the X_0 axis is coincided and reversed with the Z_{-1} axis. The distance from $\{-1\}$ to $\{0\}$ is d_0 (see Fig. 1). The coordinate frame $\{0\}$ is fixed and coordinate frame $\{-1\}$ can rotate around Z_0 an angle θ_0. The locus of the intersection of two

pipes R_1 and R_2 in the coordinate frame $\{0\}$ is given by Eq. (9), Eq. (10), Eq. (11) and (12):

$$Q_1 = \begin{bmatrix} 0 & 0 & -1 & d_0 \\ -c_0 & s_0 & 0 & 0 \\ s_0 & c_0 & 0 & 0 \\ 0 & 0 & 0 & 1 \end{bmatrix} \begin{bmatrix} x \\ y \\ z \\ 1 \end{bmatrix} = \begin{bmatrix} Q_{1x} \\ Q_{1y} \\ Q_{1z} \\ 1 \end{bmatrix}, \tag{9}$$

where

$$Q_{1x} = d_0 - \frac{-R_2 c_\varphi \pm c_{ar}\sqrt{R_1^2 - (R_2 s_\varphi)^2}}{s_{ar}}, \tag{10}$$

$$Q_{1y} = -c_0 R_2 s_\varphi \pm s_0\sqrt{R_1^2 - (R_2 s_\varphi)^2}, \tag{11}$$

$$Q_{1z} = s_0 R_2 s_\varphi \pm c_0\sqrt{R_1^2 - (R_2 s_\varphi)^2}, \tag{12}$$

s_0: $\sin\theta_0$, c_0: $\cos\theta_0$.

When cutting, pipe R_2 must be re-applied an angle $-ar^\circ$ so that the center line of R_2 coincides with Z_{-1} axis. The cutting path of pipe R_2 is given by Eq. (13), Eq. (14), Eq. (15) and Eq. (16).

$$Q_2 = \begin{bmatrix} 1 & 0 & -1 \\ 0 & c_{-ar} & -s_{-ar} \\ 0 & s_{-ar} & c_{-ar} \end{bmatrix} \begin{bmatrix} Q_{1x} \\ Q_{1y} \\ Q_{1z} \end{bmatrix} = \begin{bmatrix} Q_{2x} \\ Q_{2y} \\ Q_{2z} \end{bmatrix}, \tag{13}$$

where

$$Q_{2x} = d_0 - \frac{-R_2 c_\varphi \pm c_{ar}\sqrt{R_1^2 - (R_2 s_\varphi)^2}}{s_{ar}}, \tag{14}$$

$$Q_{2y} = c_{ar}(-c_0 R_2 s_\varphi \pm s_0\sqrt{R_1^2 - (R_2 s_\varphi)^2}) + s_{ar}(s_0 R_2 s_\varphi \pm c_0\sqrt{R_1^2 - (R_2 s_\varphi)^2}), \tag{15}$$

$$Q_{2z} = -s_{ar}(-c_0 R_2 s_\varphi \pm s_0\sqrt{R_1^2 - (R_2 s_\varphi)^2}) + c_{ar}(s_0 R_2 s_\varphi \pm c_0\sqrt{R_1^2 - (R_2 s_\varphi)^2}). \tag{16}$$

Equation (9), Eq. (10), Eq. (11), Eq. (12), Eq. (13), Eq. (14), Eq. (15) and Eq. (16) describe the paths in which the end-effector moves on them in the coordinate frame $\{0\}$ when cutting.

2.2. Cutting Direction

Beside cutting path, we must pay attention to the cutting direction. With each cutting point which many directions to go through, but only one direction is reasonable with the requirements about pipe welding conditions [3], depending on the cutting angle [4] and the position of the point, shown in Fig. 2. Cutting direction changes continuously during cutting process.

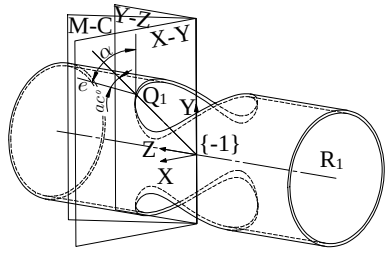

Fig. 2: Cutting direction of pipe R_1.

In the coordinate frame $\{-1\}$, plane (M, C) contains Y_{-1} axis and passes cutting point Q_1. In plane (M, C), e is the line that contains cutting direction and passes cutting point Q_1, α is the angle between e and Y_{-1} axis (given by Eq. (17) and Eq. (18)). β is the angle between plane (M, C) and (Y, Z).

$$\alpha = \widehat{Y_{-1}O_{-1}Q_1} + ac, \tag{17}$$

$$\widehat{Y_{-1}O_{-1}Q_1} = arctan2(\sqrt{Q_{1x}^2 + Q_{1z}^2}, Q_{1y}). \tag{18}$$

ac: the standard cutting angle is given before [4] (see Fig. 1 and Fig. 2).

e is found by rotating an imaginary line through Q_1 and paralleling Y_{-1} axis with an angle β around Y_{-1} axis, and then rotating this line with an angle α around Q_1. e is the line containing the direction we need.

The cutting direction in the coordinate frame $\{-1\}$ is a 3x3 matrix and given by Eq. (19):

$$H_{-1} = R_Y(\alpha)\ R_X(\beta) = \begin{bmatrix} c_\beta & s_\alpha s_\beta & c_\alpha s_\beta \\ 0 & c_\alpha & -s_\alpha \\ -s_\beta & s_\alpha c_\beta & c_\alpha c_\beta \end{bmatrix}. \tag{19}$$

From Eq. (19), we obtain the cutting direction in the coordinate frame {0} as Eq. (20):

$$H_0 = {}^{-1}_{0}R\ H_{-1} = \begin{bmatrix} s_\beta & -s_\alpha c_\beta & -c_\alpha c_\beta \\ -c_0 c_\beta & -c_0 s_\alpha s_\beta + s_0 c_\alpha & -c_0 c_\alpha s_\beta - s_0 s_\alpha \\ s_0 c_\beta & s_0 s_\alpha s_\beta + c_0 c_\alpha & s_0 c_\alpha s_\beta - c_0 s_\alpha \end{bmatrix}. \quad (20)$$

2.3. Cutting Method

There are two general cases of cutting: static pipe while moving end-effector [2] and rotating pipe while moving end-effector. Especially, the end-effector moves on a straight section with cutting direction following to Eq. (20). The combination of rotating pipe while moving end-effector on a straight section is given by Eq. (21) and Eq. (22). It will create Hyperbolic Paraboloid Pringles like the reality. This case is described in Fig. 3.

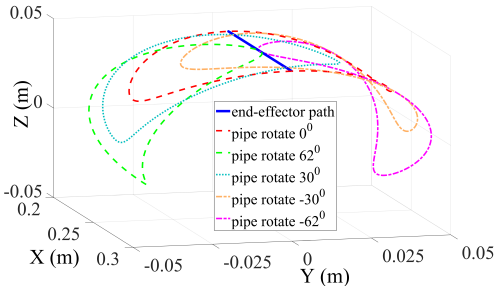

Fig. 3: The combination of rotating pipe while moving end-effector on a straight section.

Trajectory of end-effector is a parallel straight section with X_0 axis, and is located right at the top of the pipe. The straight section belongs to plane (X_0, Z_0), in which $Y_0 = 0$ and $Z_0 = R_1$. From Eq. (9), Eq. (10), Eq. (11) and Eq. (12), we infer:

$${}^{0}_{-1}Q_1 = \begin{bmatrix} d_0 - \dfrac{-R_2 c_\varphi \pm c_{ar}\sqrt{R_1^2 - (R_2 s_\varphi)^2}}{s_{ar}} \\ -c_0 R_2 s_\varphi \pm s_0\sqrt{R_1^2 - (R_2 s_\varphi)^2} \\ s_0 R_2 s_\varphi \pm c_0\sqrt{R_1^2 - (R_2 s_\varphi)^2} \end{bmatrix} = \begin{bmatrix} d_0 - \dfrac{-R_2 c_\varphi \pm c_{ar}\sqrt{R_1^2 - (R_2 s_\varphi)^2}}{s_{ar}} \\ 0 \\ R_1 \end{bmatrix}. \quad (21)$$

From Eq. (21), we obtain:

$$\theta_0 = arctan2(\mp R_2 c_\varphi, \sqrt{R_1^2 - (R_2 s_\varphi)^2}). \quad (22)$$

While the end-effector moves on a straight line in Eq. (21) with direction in Eq. (20), the pipe rotate an angle θ_0 in Eq. (22). This combination of motion will create the Hyperbolic Paraboloid Pringles in real.

3. Robot Model

The Robot model used in this paper includes 5 degrees of freedom robot arm and a degree of freedom created by the rotating motion of the pipe. This model is shown in Fig. 4.

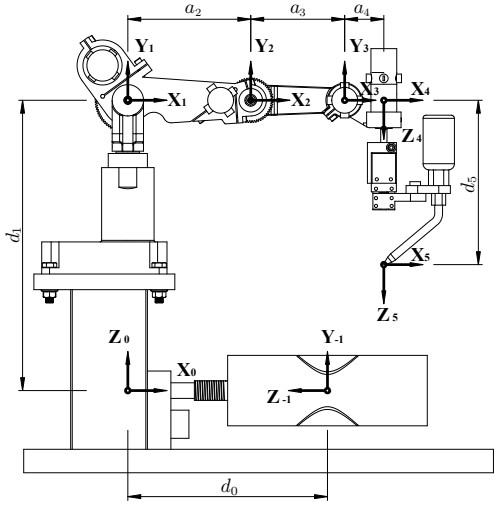

Fig. 4: The model of Robot.

3.1. Forward Kinematics

The coordinate frame {0} is the global coordinate frame of Robot system. Robot system is divided into two parts in which they combination movements together: a part includes 5 degrees of freedom robot arm and a part created by the rotating motion of a pipe. Parameters of the model are given in Tab. 1.

Based on the Denavit-Hartenberg convention, we find these transformation matrices

Tab. 1: Denavit-Hartenberg parameters of Robot.

i	α_i deg	a_i mm	d_i mm	θ_i deg	Operating range deg
0	90	0	260	θ_0	−180 to 180
1	90	0	371	θ_1	−140 to 140
2	0	157	0	θ_2	−45 to 45
3	0	120	0	θ_3	−90 to 90
4	90	50	0	θ_4	−145 to 90
5	0	0	210	θ_5	−180 to 180

${}^{0}_{-1}T$, ${}^{0}_{1}T$, ${}^{1}_{2}T$, ${}^{2}_{3}T$, ${}^{3}_{4}T$ and ${}^{4}_{5}T$. The transformation matrix ${}^{0}_{-1}T$ describe position of the pipe in global coordinate frame $\{0\}$, given by Eq. (23):

$$ {}^{0}_{-1}T = \begin{bmatrix} 0 & 0 & -1 & d_0 \\ -c_0 & s_0 & 0 & 0 \\ s_0 & c_0 & 0 & 0 \\ 0 & 0 & 0 & 1 \end{bmatrix}. \tag{23} $$

Matrix ${}^{0}_{5}T$ describes the end-effector direction and position in the coordinate frame $\{0\}$ (see [2] or [5]) is given by Eq. (24):

$$ {}^{0}_{5}T = {}^{0}_{1}T\ {}^{1}_{2}T\ {}^{2}_{3}T\ {}^{3}_{4}T\ {}^{4}_{5}T = \begin{bmatrix} n_x & a_x & o_x & p_x \\ n_y & a_y & o_y & p_y \\ n_z & a_z & o_z & p_z \\ 0 & 0 & 0 & 1 \end{bmatrix}, \tag{24} $$

where

$$ n_x = c_1c_{234}c_5 + s_1s_5, \tag{25} $$
$$ n_y = s_1c_{234}c_5 - c_1s_5, \tag{26} $$
$$ n_z = s_{234}c_5, \tag{27} $$
$$ a_x = -c_1c_{234}s_5 + s_1c_5, \tag{28} $$
$$ a_y = -s_1c_{234}s_5 - c_1c_5, \tag{29} $$
$$ a_z = -s_{234}s_5, \tag{30} $$
$$ o_x = c_1s_{234}, \tag{31} $$
$$ o_y = s_1s_{234}, \tag{32} $$
$$ o_z = -c_{234}, \tag{33} $$
$$ p_x = d_5c_1s_{234} + a_4c_1c_{234} + a_3c_1c_{23} + a_2c_1c_2, \tag{34} $$
$$ p_y = d_5s_1s_{234} + a_4s_1c_{234} + a_3s_1c_{23} + a_2s_1c_2, \tag{35} $$
$$ p_z = -d_5c_{234} + a_4s_{234} + a_3s_{23} + a_2s_2 + d_1, \tag{36} $$

s_i: $\sin\theta_i$, c_i: $\cos\theta_i$,
$s_{i\ldots k}$: $\sin(\theta_i + \cdots + \theta_k)$, $c_{i\ldots k}$: $\cos(\theta_i + \cdots + \theta_k)$.

3.2. Inverse Kinematics

Inverse kinematics results in exact positions of joints when position and direction of end-effector is known.

Equating entries (1,4) and (2,4) in the matrix (Eq. (24)), we have $\tan\theta_1$ ([2] or [6]) as Eq. (37):

$$ \frac{p_y}{p_x} = tan\theta_1. \tag{37} $$

We obtain the first angle as Eq. (38).

$$ \theta_1 = arctan2(p_y, p_x). \tag{38} $$

By multiplying s_1 and c_1 with elements (1,1), (2,1), (1,2) and (2,2) in Eq. (24) then shorten them, we find $\tan\theta_5$ as Eq (39):

$$ \frac{s_1n_x - c_1n_y}{s_1o_x - c_1o_y} = \tan\theta_5. \tag{39} $$

Infer θ_5 as Eq (40):

$$ \theta_5 = arctan2(s_1n_x - c_1n_y, s_1o_x - c_1o_y). \tag{40} $$

To find θ_3, we need to find $\theta_{234} = \theta_2 + \theta_3 + \theta_4$. Equating entries (1,3), (2,3) and (3,3) in the matrix Eq. (24), we obtain Eq (41):

$$ \frac{c_1a_x + s_1a_y}{-a_z} = \tan\theta_{234}. \tag{41} $$

Infer θ_{234} as Eq (42):

$$ \theta_{234} = arctan2(c_1a_x + s_1a_y, -a_z). \tag{42} $$

After we have θ_1 and θ_5, we calculate the value of the transformation matrix ${}^{0}_{1}T$ and ${}^{4}_{5}T$. Based on the value of the transformation matrix ${}^{0}_{1}T$, we find ${}^{1}_{4}T$ as Eq. (43):

$$ {}^{1}_{4}T = {}^{0}_{1}T^{-1}\ {}^{0}_{5}T\ {}^{4}_{5}T^{-1} = \begin{bmatrix} c_{234} & 0 & s_{234} & a_4c_{234} + a_3c_{23} + a_2c_2 \\ s_{234} & 0 & -c_{234} & a_4s_{234} + a_3s_{23} + a_2s_2 \\ 0 & 1 & 0 & 0 \\ 0 & 0 & 0 & 1 \end{bmatrix}. \tag{43} $$

We set:

$$ \begin{cases} x_{41} = a_4c_{234} + a_3c_{23} + a_2c_2, \\ y_{41} = a_4s_{234} + a_3s_{23} + a_2s_2. \end{cases} \tag{44} $$

Rearranging the two equations in Eq. (44), squaring them and then adding the squares gives Eq. (45) and Eq. (46):

$$c_3 = \frac{(x_{41} - a_4 c_{234})^2 + (y_{41} - a_4 s_{234})^2 - a_3^2 - a_2^2}{2a_3 a_2}, \tag{45}$$

$$s_3 = \pm\sqrt{1 - c_3^2}. \tag{46}$$

Infer θ_3 as Eq (47):

$$\theta_3 = arctan2(s_3, c_3). \tag{47}$$

Set:

$$\begin{cases} k_1 = a_3 c_3 + a_2, \\ k_2 = a_3 s_3. \end{cases} \tag{48}$$

From Eq. (44) and Eq. (48), we obtain:

$$\begin{cases} x_{41} - a_4 c_{234} = k_1 c_2 - k_2 s_2, \\ y_{41} - a_4 s_{234} = k_1 s_2 + k_2 c_2. \end{cases} \tag{49}$$

Set:

$$\begin{cases} k_3 = \sqrt{k_1^2 + k_2^2}, \\ \gamma = arctan2(k_2, k_1). \end{cases} \tag{50}$$

Based on Eq. (49) and Eq. (50), we obtain Eq. (51).

$$\begin{cases} \cos(\gamma + \theta_2) = \dfrac{x_{41} - a_4 c_{234}}{k_3}, \\ \sin(\gamma + \theta_2) = \dfrac{y_{41} - a_4 s_{234}}{k_3}. \end{cases} \tag{51}$$

From Eq. (51), we obtain θ_2 ([2] or [7]) as Eq. (52):

$$\theta_2 = arctan2(y_{41} - a_4 s_{234}, x_{41} - a_4 c_{234}) - arctan2(k_2, k_1). \tag{52}$$

And we have θ_4 as Eq. (53):

$$\theta_4 = \theta_{234} - \theta_3 - \theta_2. \tag{53}$$

3.3. Trajectory Planning

Links will be moved concurrently and corporately so that end-effector will follow cutting equation in defined duration t.

In Cartesian space, cutting path will be divided into set of points in which the space between these points is very small and equal Δp. Inverse kinematics is used to define joint variables in joint space corresponding to set of points in Cartesian space ([8], [9] or [10]).

Joint path planning must ensure the continuity of position, velocity, acceleration and cubic polynomial is a suitable choice.

Suppose that n^{th} joint rotates angles θ_i and θ_{i+1} in durations t_k and t_{k+1} respectively, the cubic polynomial of the form of n^{th} joint:

$$\theta_i(t) = a_{i3} t^3 + a_{i2} t^2 + a_{i1} t + a_{i0}. \tag{54}$$

Velocity:

$$\dot{\theta}_i(t) = 3a_{i3} t^2 + 2a_{i2} t + a_{i1}. \tag{55}$$

Parameters of the cubic polynomial must be defined based on constraints so that joint path satisfy the continuity of position, velocity and acceleration.

Position constraints:

$$\theta_i(0) = \theta_{k-1}, \tag{56}$$

$$\theta_i(t_k) = \theta_{i+1}(0) = \theta_k, \tag{57}$$

$$\theta_{i+1}(t_{k+1}) = \theta_{k+1}. \tag{58}$$

Velocity constraints:

$$\dot{\theta}_i(0) = \dot{\theta}_{k-1}, \tag{59}$$

$$\dot{\theta}_i(t_k) = \dot{\theta}_{i+1}(0) = \dot{\theta}_k, \tag{60}$$

$$\dot{\theta}_{i+1}(t_{k+1}) = \dot{\theta}_{k+1}. \tag{61}$$

Acceleration constraints:

$$\ddot{\theta}_i(t_k) = \ddot{\theta}_{i+1}(0) = \ddot{\theta}_k. \tag{62}$$

The durations are equal: $t_k = t_{k+1} = \Delta t$, solving Eq. (56), Eq. (57), Eq. (58), Eq. (59), Eq. (60), Eq. (61) and Eq. (62), we obtain:

$$a_{i3} = \frac{-2(\theta_k - \theta_{k-1}) + (\dot{\theta}_k + \dot{\theta}_{k-1})\Delta t}{\Delta t^3}, \tag{63}$$

$$a_{i2} = \frac{6(\theta_k - \theta_{k-1}) - 2(\dot{\theta}_k + 2\dot{\theta}_{k-1})\Delta t}{2\Delta t^2}, \tag{64}$$

$$a_{i1} = \dot{\theta}_{k-1}, \tag{65}$$

$$a_{i0} = \theta_{k-1}. \tag{66}$$

Plugging Eq. (63), Eq. (64), Eq. (65) and (66) into Eq. (54) and Eq. (55), we find that:

$$\theta_i(t) = \frac{-2(\theta_k - \theta_{k-1}) + (\dot{\theta}_k + \dot{\theta}_{k-1})\Delta t}{\Delta t^3} t^3 + \frac{6(\theta_k - \theta_{k-1}) - 2(\dot{\theta}_k + 2\dot{\theta}_{k-1})\Delta t}{2\Delta t^2} t^2 + \dot{\theta}_{k-1} t + \theta_{k-1}, \quad (67)$$

$$\dot{\theta}_i(t) = 3\frac{-2(\theta_k - \theta_{k-1}) + (\dot{\theta}_k + \dot{\theta}_{k-1})\Delta t}{\Delta t^3} t^2 + 2\frac{6(\theta_k - \theta_{k-1}) - 2(\dot{\theta}_k + 2\dot{\theta}_{k-1})\Delta t}{2\Delta t^2} t + \dot{\theta}_{k-1}. \quad (68)$$

4. Simulation and Control

Trajectory and direction were planned in Cartesian space. They will be transformed into the joint space. The robot is controlled in the joint space so that the end-effector follows the trajectory and the expected direction. Control flow chart algorithm is given by Fig. 5.

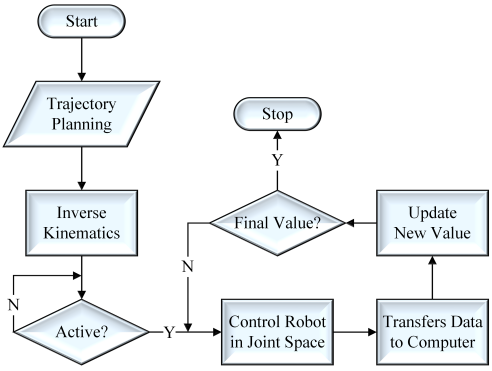

Fig. 5: Control flowchart algorithm.

The robot is drawn by SolidWorks as Fig. 6. This Robot system is imported into Matlab Simulink as Fig. 7.

PID transfer function of the first order filter ([11] and [12]) is given by Eq. (69):

$$\frac{V(s)}{E(s)} = \frac{K_d s + K_p + \frac{K_i}{s}}{\tau_f s + 1} = \frac{\frac{K_d}{\tau_f} s^2 + \frac{K_p}{\tau_f} s + \frac{K_i}{\tau_f}}{s^2 + \frac{s}{\tau_f}}, \quad (69)$$

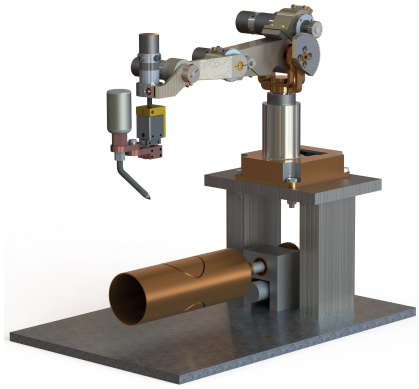

Fig. 6: The 3D system of Robot.

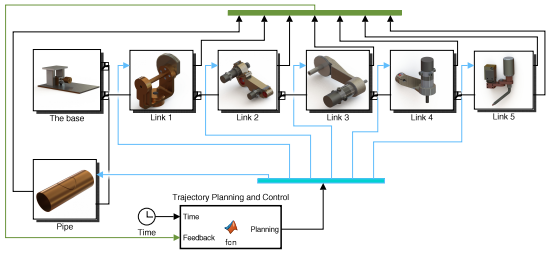

Fig. 7: The Robot system in Matlab Simulink.

where

- V: The output of the controller,
- E: Error between the input value and the feedback value,
- K_p, K_d, K_i: Proportional gain, derivative gain, integral gain and
- τ_f: The time constant of the first order filter.

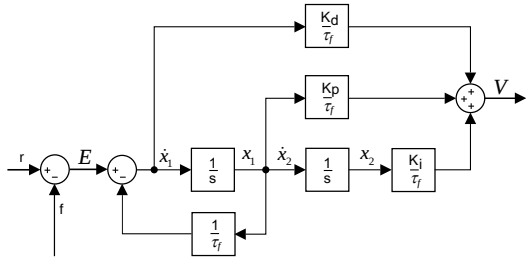

Fig. 8: PID controller with first order filter.

From Fig. 8, we have:

$$\dot{x}_1 = -\frac{1}{\tau_f}x_1 + e, \tag{70}$$

$$\dot{x}_2 = x_1, \tag{71}$$

$$V = \frac{K_i}{\tau_f}x_2 + \frac{K_p}{\tau_f}x_1 + \frac{K_d}{\tau_f}\dot{x}_1 = \left(\frac{K_p}{\tau_f} - \frac{K_d}{\tau_f^2}\right)x_1 + \frac{K_i}{\tau_f}x_2 + \frac{K_d}{\tau_f}e. \tag{72}$$

In state space, Eq. (70), Eq. (71) and Eq. (72) are given by Eq. (73) and Eq. (74):

$$\begin{bmatrix}\dot{x}_1\\ \dot{x}_2\end{bmatrix} = \begin{bmatrix}-\frac{1}{\tau_f} & 0\\ 1 & 0\end{bmatrix}\begin{bmatrix}x_1\\ x_2\end{bmatrix} + \begin{bmatrix}1\\ 0\end{bmatrix}e, \tag{73}$$

$$V = \begin{bmatrix}\frac{K_p}{\tau_f} - \frac{K_d}{\tau_f^2} & \frac{K_i}{\tau_f}\end{bmatrix}\begin{bmatrix}x_1\\ x_2\end{bmatrix} + \frac{K_d}{\tau_f}e. \tag{74}$$

Set:

$$X = \begin{bmatrix}x_1\\ x_2\end{bmatrix}; \qquad \dot{X} = \begin{bmatrix}\dot{x}_1\\ \dot{x}_2\end{bmatrix}, \tag{75}$$

$$A = \begin{bmatrix}-\frac{1}{\tau_f} & 0\\ 1 & 0\end{bmatrix}; \qquad B = \begin{bmatrix}1\\ 0\end{bmatrix}, \tag{76}$$

$$C = \begin{bmatrix}\frac{K_p}{\tau_f} - \frac{K_d}{\tau_f^2} & \frac{K_i}{\tau_f}\end{bmatrix}; \qquad D = \frac{K_d}{\tau_f}. \tag{77}$$

From Eq. (75), Eq. (76) and Eq. (77), we find that:

$$\dot{X} = AX + Be, \tag{78}$$

$$V = CX + De. \tag{79}$$

The simulated results:

The simulation time is the 30 s. Figure. 9 and Fig. 10 give trajectory and response of six joints in the joint space.

Figure 11 and Fig. 12 are the error graphs of six joints in the joint space. In Fig. 11: Since the static pipe leads to the joint 0 is motionless and errorless, the maximum error belongs to joints 3, 4 and 5 with a maximum value of 0.04°. The best activity is joint 1 with a maximum error of 0.0075°. In Fig. 12: Since the end-effector moves on the straight section, joint 1 stays still.

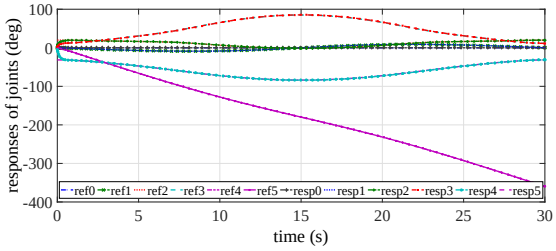

Fig. 9: Trajectory and response of six joints in the case of static pipe.

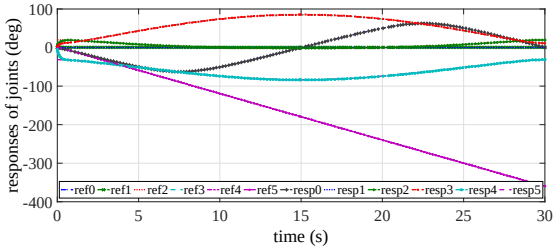

Fig. 10: Trajectory and response of six joints in the case of rotary pipe.

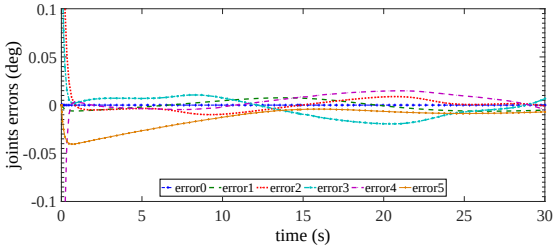

Fig. 11: Joint errors of six joints in the case of static pipe.

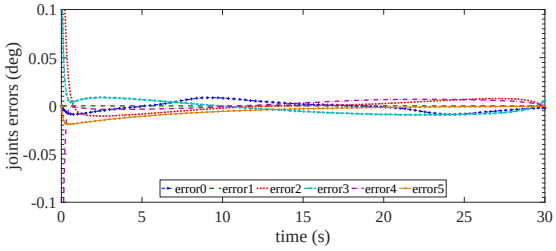

Fig. 12: Joint errors of six joints in the case of rotary pipe.

The maximum error belongs to joint 3 with a value of 0.009°. The best activity is joint 4 with a maximum error of 0.0006°.

Figure 13 and Fig. 14 are the error graphs of the end-effector in the three axes of $X-Y-Z$ in the Cartesian space corresponding to two cases: standing and rotating. In Fig. 13: Position error

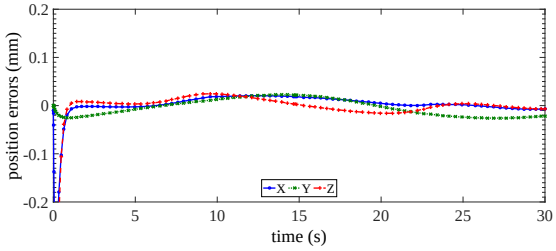

Fig. 13: Position errors of the end-effector in the case of static pipe.

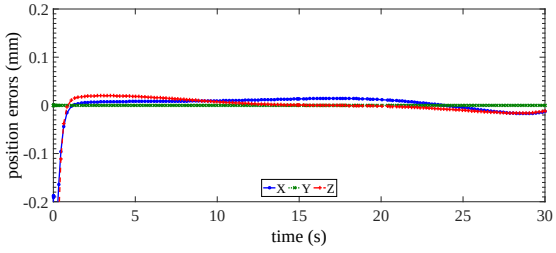

Fig. 14: Position errors of the end-effector in the case of rotary pipe.

ranges from -0.022 to 0.026 mm. In Fig. 14: Position error ranges from -0.021 to 0.020 mm.

Discussion: The simulated results showed that the case of a static pipe cutting was not as good as the case of a rotary pipe cutting.

5. Experiment

Figure 15 is the real robot system. Time to finishing work of Robot is set to 30 s. Two microcontrollers will control five harmonic driver motors corresponding to five joints of Robot and a rotary motor. Data obtained from Robot will be transmitted to the computer.

The experimental results:

Figure 16 and Fig. 17 are the error graphs of six joints in the joint space. In Fig. 16: The maximum error belongs to joints 3 and 4; the error ranges from $-0.072°$ to $0.079°$. In Fig. 17: The maximum error belongs to joints 3 and 4; the error ranges from $-0.058°$ to $0.045°$. These errors are smaller in Fig. 16.

Figure 18 and Fig. 19 are the error graphs of the end-effector in the three axes of $X-Y-Z$ in the Cartesian space corresponding to two cases:

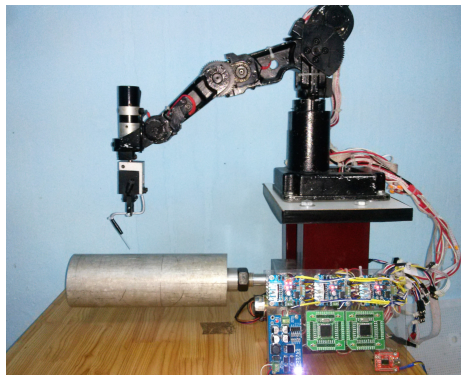

Fig. 15: Experimental Robot system.

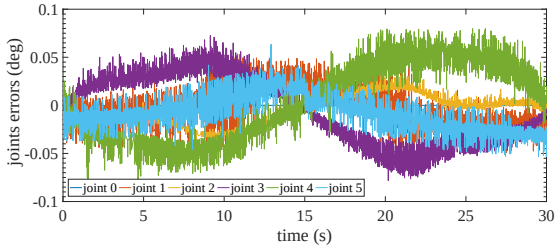

Fig. 16: Joint errors of six joints in the case of static pipe.

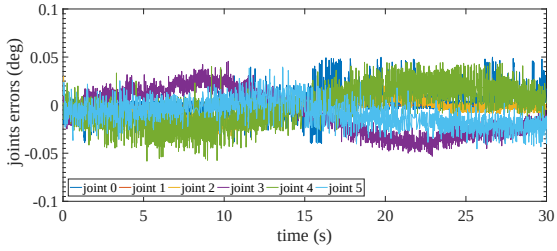

Fig. 17: Joint errors of six joints in the case of rotary pipe.

standing and rotating. We see that the errors in the two graphs range from -0.2 to 0.2 mm. Fig. 18 has a larger error graph and is more oscillating than Fig. 19.

Discussion: The experimental results showed that the case of a rotary pipe cutting was better than the case of a static pipe cutting, with less error and less oscillation error.

6. Conclusion

The paper has solved the whole problem: building the cutting trajectory, solving the inverse

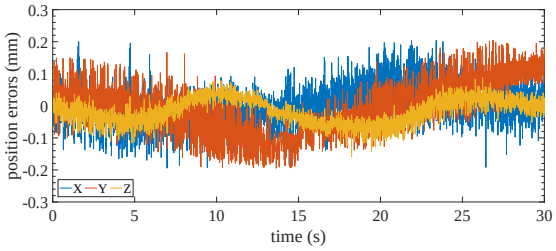

Fig. 18: Position errors of the end-effector in the case of static pipe.

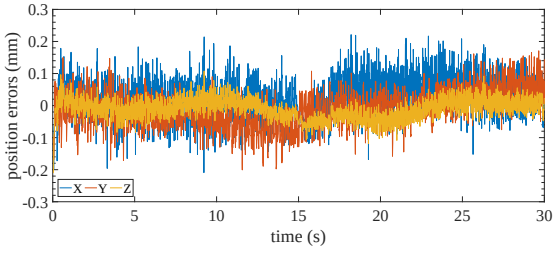

Fig. 19: Position errors of the end-effector in the case of rotary pipe.

kinematics, planning the trajectory of motion, simulating and controlling Robot in reality. More importantly, this paper has developed two different pipe cutting solutions, and gives the comparative results between the two ones in both simulation and experiment. These comparative results show that method of the end-effector moves on a straight line while the rotating pipe to create the cutting path and direction for better than method of the end-effector moves on cutting path and direction while the stationary pipe. This conclusion is an important note that we should design the robot arm and the pipe coordinate movement together, bring the best effect.

Acknowledgment

The work was supported by Professor Ivan Zelinka, Ton Duc Thang University and Professor Nguyen Tan Tien, "Hi-Tech Mechatronics Laboratory" Ho Chi Minh City University of Technology.

References

[1] MOHARANA, B., R. GUPTA and B. K. KUSHWAHA. Optimization and Design of a Laser-Cutting Machine using Delta Robot. *International Journal of Engineering Trends and Technology*. 2014, vol. 10, no. 4, pp. 176–179.

[2] QUOC BAO, D., T. T. PHAN and T. T. NGUYEN. Study on Control of Pipe Cutting Robot. In: *International Symposium on Mechatronics and Robotics*. Ho Chi Minh City: HCMUT, 2013, pp. 118–123.

[3] Chapter 2. MCALLISTER, E. W. *Pipeline Rules of Thumb Handbook*. 8th Edition. Boston: Elsevier/Gulf Professional Publishing, 2014, pp. 64–91. .

[4] Chapter 17. MENON, E. S. *Pipeline Planning and Construction Field Manual*. Waltham: Gulf Professional Publishing, 2011, pp. 357–378.

[5] VERMA, A. and V. A. DESHPANDE. End-effector position analysis of SCORBOT-ER-Vplus Robot. *International Journal of Smart Home*. 2011, vol. 5, no. 1, pp. 1–6.

[6] DESHPANDE, V. A. and P. M. GEORGE. Analytical solution for inverse kinematics of SCORBOT-ER-Vplus Robot. *International Journal of Emerging Technology and Advanced Engineering*. 2012, vol. 2, iss. 3, pp. 478–481.

[7] XU, D., C. A. ACOSTA CALDERON, J. Q. GAN, H. HU and M. TAN. An analysis of the inverse kinematics for a 5-DOF manipulator. *International Journal of Automation and Computing*. 2005, vol. 2, iss. 2, pp. 114–124.

[8] JAZAR, R. N. *Theory of Applied Robotics: Kinematics, Dynamics, and Control*. 2nd Edition. New York: Springer, 2010.

[9] CRAIG, J. J. *Introduction to Robotics: Mechanics and Control*. 3rd Edition. Upper Saddle River: Pearson/Prentice Hall, 2005.

[10] TONDU, B. and S. A. BAZAZ. The Three-Cubic Method: An Optimal Online Robot Joint Trajectory Generator under Velocity, Acceleration, and Wandering Constraints. *The International Journal of Robotics Research*. 1999, vol. 18, iss. 9, pp. 893–901.

[11] SKOGESTAD, S. Simple Analytic Rules for Model Reduction and PID Controller Tuning. *Journal of Process Control*. 2003, vol. 13, iss. 4, pp. 291–309.

[12] AGRAWAL, S., V. KUMAR, K. P. S. RANA and P. MISHRA. Optimization of PID controller with first order noise filter. In: *International Conference on Futuristic Trends on Computational Analysis and Knowledge Management*. Noida: IEEE, 2015, pp. 226–231.

About Authors

Quoc Bao DIEP received the M.Sc. degree from Ho Chi Minh City University of Technology. He is a Ph.D. student at the Faculty of Electrical Engineering and Computer Science, VSB–Technical University of Ostrava. His research interests include industrial robot, 3D simulation, and intelligent control.